Scilight

Journal of Innovations in Materials and Manufacturing Engineering
https://www.sciltp.com/journals/jimme

Article

Evaluating the Ability of Additively Manufactured Polyester Blends to Thermally Recover from Organic Chemical Exposure

Katia Lizbeth Delgado Ramos [1,2], Stephanie Moreno [1,2], Osvaldo Bustamante [1,2] and David A. Roberson [1,2,*]

[1] Polymer Extrusion Lab, The University of Texas at El Paso, El Paso, TX 79968, USA
[2] Department of Metallurgical, Materials and Biomedical Engineering, The University of Texas at El Paso, El Paso, TX 79968, USA
* Correspondence: droberson@utep.edu

How To Cite: Delgado Ramos, K.L.; Moreno, S.; Bustamante, O.; et al. Evaluating the Ability of Additively Manufactured Polyester Blends to Thermally Recover from Organic Chemical Exposure. *Journal of Innovations in Materials and Manufacturing Engineering* **2026**, *1*(1), 2.

Received: 6 October 2025
Revised: 19 November 2025
Accepted: 21 November 2025
Published: 26 November 2025

Abstract: The work presented here sought to understand if damage induced to polymeric materials by chemical exposure could be mitigated by thermal annealing. This concept has not been widely explored in literature. Here, two polymer blends with known shape memory properties and documented thermal process for shape recovery; a binary blend of equal parts by mass polycaprolactone (PCL)/thermoplastic urethane (TPU), and a ternary mixture of equal parts by mass polycaprolactone (PCL), thermoplastic urethane (TPU), and polylactic acid (PLA) were subjected to chemical exposure to either ethyl acetate or heated acetic acid for a duration of 7 days. The specimens were fabricated by fused filament fabrication (FFF) in two different raster orientations. Swell testing revealed a dependence on raster orientation for solvent uptake. Characterization of the chemical bonds by FTIR-ATR revealed the acetic acid exposure to be more damaging in terms of breaking of chemical bonds and that thermal recovery reforms some bonds. Analysis of tensile test results with Tukey-Kramer Honestly Significant Difference revealed thermally annealing specimens after chemical exposure could recover mechanical properties to a level similar to specimens that were not exposed. Analysis by scanning electron microscopy revealed that the chemical attack was concentrated at the print raster interface, leading to delamination between the print rasters. Analysis by way of DMA revealed that chemical exposure lowered the max tan δ value, but not the temperature at which this parameter was reached as compared to control specimens. This work demonstrates that thermally induced recovery can heal chemical damage to polymer materials, offering a route to extend the life of plastic parts and reduce polymer waste.

Keywords: chemical degradation of polymers; additive manufacturing; self-healing polymers; fused filament fabrication; materials characterization; mechanical properties

1. Introduction

Evidence of the detrimental impact of environmental polymeric waste, particularly in the form of micro and nano plastics grows daily. From detection of microplastics in oceanic fauna [1,2] to detection in human tissues, fluids, and fecal matter [3–7], our society needs a solution to the problem of polymeric waste. A potential path to a solution that has been explored by our group has been the development of polymers blends that can be recovered from mechanical damage, and we have also proposed a "resilience parameter" as a physical property that quantifies the capacity of polymers with shape memory properties to retain strength after thermal recovery from plastic

deformation [8]. The premise behind implementing resilient polymeric materials is that if a plastic component can be healed from damage to the point where it can be used again rather than be thrown away, the reduction in waste would be twofold in that the broken component would not be thrown away and new material would not be used as a replacement component. The shape recovery process has been the key driver for recovery from plastic deformation and it is well-known that an element of the overall self-healing ability of a given polymer is its shape memory properties [9,10].

The fabrication of polymer blends with the end goal of manipulating the shape memory properties of a material has been demonstrated in literature by our group and others, with example blend constituents being polylactic acid (PLA) blended with elastomers such as thermoplastic urethane (TPU), polyamide elastomer (PAE), and styrene ethylene butylene styrene (SEBS) [11–16] and blends composed of polycaprolactone (PCL) and TPU [17–20]. The work presented here builds upon a previous study performed by our group [21] that characterized the microstructure and shape memory properties of binary PCL/TPU blends and ternary PCL/TPU/PLA blends in the context of 4D printing, and found that the process of plastic deformation followed by thermal recovery led to a strengthening effect in the PCL/TPU blend that was driven by formation of crystalline domains. This initial characterization effort was carried on by another study by Delgado Ramos, et al. [22] that found these blend systems to have a marginal ability to recover from a partial cut, which is damage beyond plastic deformation.

Typically, the self-healing ability of a polymeric material is characterized by way of a cut test of a tensile specimen where the equations to evaluate the self-healing efficiency (R) is calculated by comparing the mechanical properties, namely ultimate tensile strength (UTS, denoted as σ), Young's modulus (E), and maximum % elongation (ε) of pristine specimens to those that were subjected to a cut test as proposed by Wool and O'Connor [23] and based on the equations below:

$$R(\sigma) = \frac{\sigma_{cut}}{\sigma_{pristine}} \cdot 100\% \quad (1)$$

$$R(E) = \frac{E_{cut}}{E_{pristine}} \cdot 100\% \quad (2)$$

$$R(\varepsilon) = \frac{\varepsilon_{cut}}{\varepsilon_{pristine}} \cdot 100\% \quad (3)$$

Rather than characterizing the self-healing efficiency, in the work presented in this study we explored the ability of the binary and ternary polyester blends originally presented in Lares Carillo, et al. [21] to recover from damage caused by exposure to organic chemicals.

While polymers that can recover from mechanical damage have been characterized in literature [9,23–27] polymer systems that heal from chemical damage are not as common. One example of a polymer system with the ability to heal from chemical damage was demonstrated by Fu, et al. [28] however, this system was a composite mixture of poly(dimethylsiloxane) (PDMS) foam, halite (table salt), and multi-walled carbon nanotubes (MWCNTs). The work presented here is novel in terms of its rarity and simplicity. Effectively, we characterized the ability of our polymer blends to recover from chemical damage rather than mechanical damage. The method of recovery was thermal annealing. Additively manufactured test coupons were exposed to one of two organic chemicals, glacial acetic acid, and ethyl acetate. These two chemicals were chosen because glacial acetic acid is known to dissolve PCL [29] and degrade PLA [30]. Moreover, acetic acid has been demonstrated as a component in the chemical recycling of polyurethanes due to its ability to sever the urethane segment [31]. Additionally, ethyl acetate is known to attack PCL, TPU, and PLA [32–34].

The effect of chemical exposure and the effect of a thermal annealing process on exposed specimens was evaluated through different materials characterization techniques: tensile testing, swelling measurements, scanning electron microscopy (SEM) to analyze the fracture surface of tensile specimens, and finally Fourier-transform infrared spectroscopy in attenuated total reflectance mode (FTIR-ATR), to understand the role of individual bonds. The impact of raster pattern orientations 0° and 45° was also analyzed to determine if there was any impact on solvent-induced degradation. This research aims to determine if the same thermal recovery process used to recover the programed geometry of a shape memory polymer can be used to mitigate solvent damage.

2. Materials and Methods

The blends used in this study were the same polyester blends used in our previous works [21,22] where one blend was a 50:50 by mass mixture of PCL and TPU and the other was a three part (equal parts by mass) compound of PCL, TPU and PLA. As described in previous works involving these blends [21,22], the TPU used was

NinjaFlex 3D printer filament (Natural color, Fenner Precision Polymers, Lititz, PA, USA), PCL pellets were supplied by Polly Plastics (Midland, MI, USA), and the PLA used was Ingeo Biopolymer pellets Grade 4043D from NatureWorks, LLC (Minnetonka, MN, USA). To facilitate melt compounding, the TPU was pelletized. The equipment used to create TPU pellets was a Collin strand pelletizer (Model SP1, Collin Lab & Pilot solutions, Norcross, GA, USA). The TPU was then dried at a temperature of 50 °C for a duration of 3 h in a horizontal airflow oven (Model 1370FM, VWR International, West Chester, PA, USA). The PLA and PCL pellets were dried in a compressed air dryer (Micro Dryer CAFM station, Dri-Air Industries, East Windsor, CT, USA). The PLA was dried for 4 h at 80 °C while the PCL pellets were dried for 2 h at 50 °C.

The pellets were then manually mixed in plastic bags. The mixtures were then fed to a twin-screw extruder compounder (Model ZK 25-T, Collin Lab & Pilot Solutions, Norcross, GA, USA) using the same parameters reported in Lares Carrillo, et al. and Delgado Ramos, et al. [21,22]. The compounded materials were converted to a filament with a diameter compatible with most fused filament fabrication (FFF) 3D printers, 1.75 mm. The extruded filament was then used to fabricate tensile samples following the geometry for the Type V specimen as described in the ASTM D638 standard for the tensile testing of plastics [35]. Rectangular specimens were also fabricated for dynamic mechanical analysis (DMA) based on the ASTM E1640 standard [36]. The specimens were made using a Creality Ender 3 S1 Pro FFF machine (Shenzhen Creality 3D Technology Co., Ltd., Shenzhen, China). In order to determine if aspects related to additive manufacturing had an influence on the interaction between material and solvent, two raster patterns were used (Figure 1): a raster pattern with alternating layers of 45° (Figure 1a), and a raster pattern (designated as 0°) where the print beads were deposited in a direction coincident with the length of the specimen (Figure 1b). The machine parameters used to fabricate the specimens in this study are listed in Table 1.

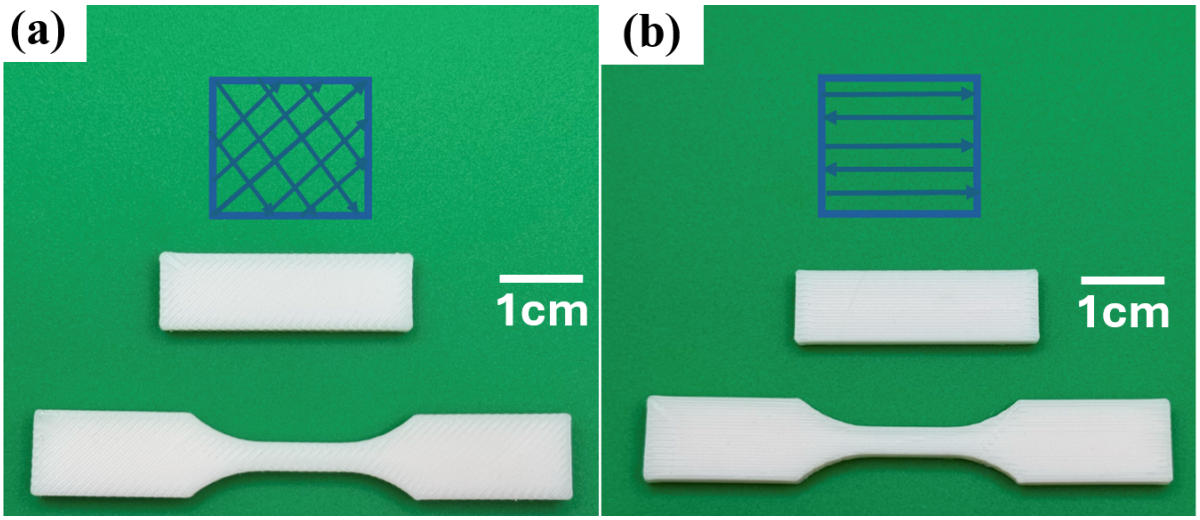

Figure 1. Example of FFF-made specimens fabricated in (**a**) a 45° raster pattern and (**b**) a 0° raster pattern.

Table 1. Machine settings for the FFF machine used in this study.

Print Parameter	PCL/TPU	PCL/TPU/PLA
Bed Temperature (°C)	60	70
Nozzle Temperature (°C)	190	200
Nozzle Diameter (mm)	0.4	0.4
Retraction distance (mm)	8	10
Extrusion Multiplier	1.05	1.05
Layer Height (mm)	0.2	0.2
Print Speed (mm/min)	1600	1600
Infill Percentage (%)	100	100

For the chemical testing, glacial acetic acid (ACS grade) was acquired from VWR International (Radnor, PA, USA) and ethyl acetate (99.5% ACS reagent grade) was obtained from Sigma Aldrich, Inc. (St. Louis, MO, USA). Twelve Type V tensile specimens, six with a 45° raster pattern and six with 0° raster pattern, from each polymer blend were weighed before exposure. Additionally, eight specimens for dynamic mechanical analysis (DMA) were included. The specimens were divided and half were placed in a sealed glass container containing glacial acetic acid which was then positioned on a hot plate that was set to a temperature of 60 °C without stirring for 7 days. The reason

we chose these experimental parameters for the acetic acid exposure was because we used the same parameters for exposing PLA and PLA-wood composite specimens to food-grade acetic acid in a previous work [37]. The remaining specimens were exposed to ethyl acetate in a sealed glass container at room temperature for 7 days. We chose not to heat the ethyl acetate due to flammability concerns. We acknowledge that the addition of elevated temperature to the acetic acid pool negates a direct comparison between the effect of acetic acid and ethyl acetate. After the exposure period, all samples were gently blot dried with a paper towel and allowed to sit for 24 h in ambient conditions and then reweighed with a laboratory balance as described in a previous work by our group [37].

Calculation of the swelling percentage of the individual specimens was determined by measuring the mass gained after exposure, with the following equation [38]:

$$Swell\ \% = \left(\frac{m_1 - m_0}{m_0}\right) \times 100 \quad (4)$$

where m_1 is the mass after 7 days of exposure followed by 24 h of drying in ambient conditions, and m_0 is the initial mass of the specimen before exposure.

Following the mass measurements, six samples from each blend and raster orientation were subjected to tensile testing until failure, which was conducted using an MTS Criterion C-44 tensile testing machine with an Advantage™ Model AHX 800 extensometer (MTS Systems Corporation, Eden Prairie, MN, USA). The remaining six samples were thermally recovered by placing them in the same horizontal airflow oven used to dry the TPU pellets at a temperature of 65 °C for a duration of 5 min. The temperature for recovery was determined by DMA characterization performed previously by our group that determined the recovery temperature based on the temperature at which the maximum tan δ is observed [21]. After the thermal recovery process, the samples were removed from the oven and left to cool in ambient conditions. The recovered specimens were then tested in the tensile test machine to evaluate any changes in mechanical performance.

In addition to the mechanical test, the samples were characterized with a Nicolet iS5 FTIR instrument equipped with an iD7 ATR Diamond accessory (ThermoFisher Scientific, Waltham, MA, USA). The fracture surfaces of used tensile test specimens were analyzed by SEM (Model SU-3500, Hitachi America, Ltd., New York, NY, USA). To facilitate analysis of non-conductive specimens, the SEM was operated in variable pressure mode with an acceleration voltage of 15 kV. Additionally, images were obtained using an ultra-variable detector (UVD) which generates images analogous to a secondary electron (SE) signal in a low-pressure mode. Finally, DMA was carried out using a PerkinElmer DMA 8000 (PerkinElmer, Waltham, MA, USA) operating in dual cantilever mode at a frequency of 1 Hz over a temperature range of −70 °C to 100 °C.

3. Results and Discussion

3.1. Swell Test

As shown in Figure 2, the swelling behavior indicates a significant variation depending on which liquid media the specimens were exposed to. Most noteworthy is the PCL/TPU specimens exposed to acetic acid exhibited as a negative swelling result indicating mass loss. This mass loss was likely accelerated due to the addition of heat as thermal energy can increase the reactivity of acetic acid [39]. The 45° raster pattern specimens exhibited a higher negative swelling at −17.65 ± 11.69% compared to −3.57 ± 1.86% for the 0° raster pattern for specimens. Residue was found in the containers that were used for exposure. The residue was recovered, weighed and subjected to analysis by way of FTIR-ATR, and the results will be discussed below. PCL/TPU specimens exposed to ethyl acetate exhibited positive swelling, with the specimens fabricated in the 0° raster pattern exhibiting a lower percentage of swelling, 1.80 ± 0.59% compared to 2.53 ± 4.16% for the specimens fabricated in the 45° raster pattern. In the case of the PCL/TPU blend, the 45° raster pattern appears to be more susceptible to exposure to the liquid media explored in this study.

In contrast, PCL/TPU/PLA exhibited consistent positive swelling when exposed to either acetic acid or ethyl acetate at the elevated temperature of 60 °C. The PCL/TPU/PLA fabricated in the 45° raster pattern and exposed to acetic acid exhibited the highest positive swelling at 9.46 ± 7.33%. Again, this is lower than the % swelling for the specimens fabricated in a 0° raster pattern (1.53 ± 1.41%). The difference in swelling behavior associated with raster pattern was also observed for specimens exposed to ethyl acetate with specimens fabricated in the 0° raster pattern swelling by 3.89 ± 0.48% and those fabricated in a 45° pattern exhibiting a %swelling of 4.68 ± 1.26%. For both blends and solvents, the 0° raster pattern was less susceptible to exposure. The reason for the difference is most-likely related to voids within the printed specimen as work involving the effect of moisture absorption performed by Kim et al. demonstrated a dependence on print raster and orientation for mass gained by ABS specimens manufactured by fused deposition modeling (FDM™) and immersed in distilled water [40]. As seen in

Figure 1, the 45° raster pattern is made of alternating layers effectively creating a web-like geometry, which has a higher propensity to form voids as compared to the 0° waster pattern which is essentially like stacked rods. Swell test results are listed in Table 2.

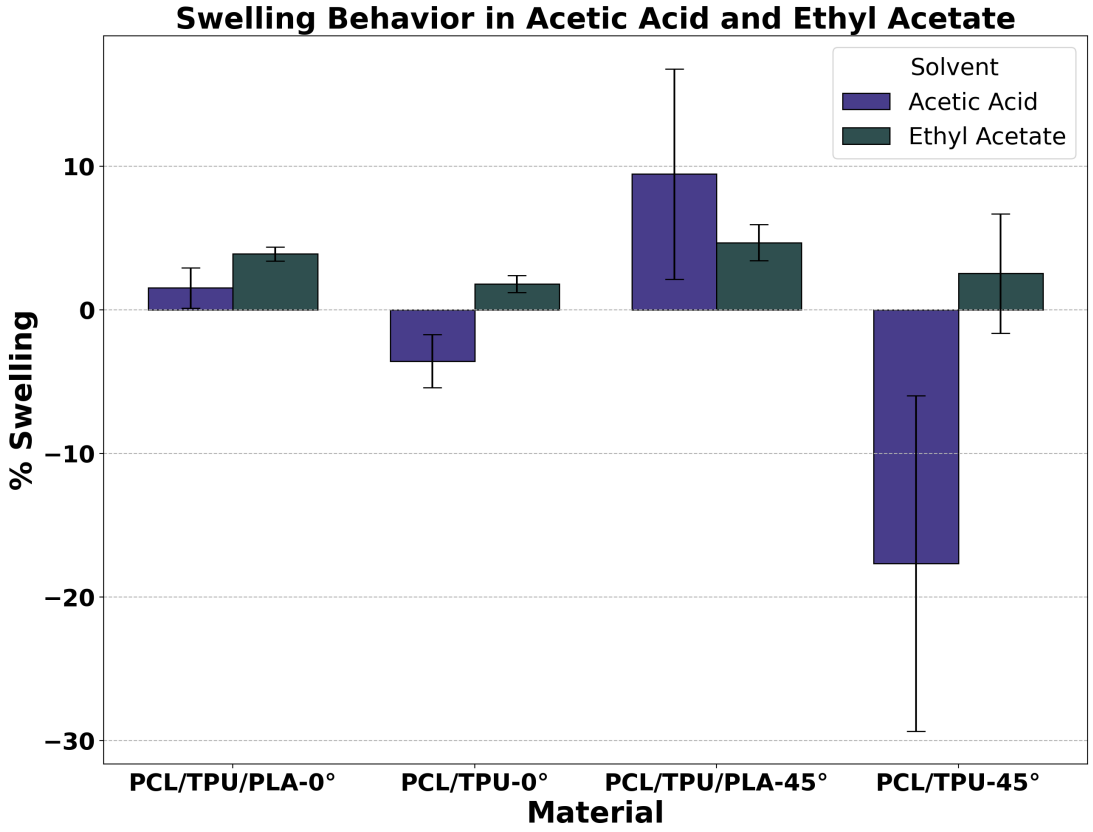

Figure 2. Swelling percentage of the polymer blends, fabricated in different raster patterns that were exposed to either acetic acid or ethyl acetate.

Table 2. Swell Test Results.

	Acetic Acid		Ethyl Acetate	
Sample Type	**% Swelling**	**σ**	**% Swelling**	**σ**
PCL/TPU/PLA-0°	1.53	1.41	3.89	0.48
PCL/TPU-0°	−3.57	1.86	1.80	0.59
PCL/TPU/PLA-45°	9.46	7.33	4.68	1.26
PCL/TPU-45°	−17.65	11.69	2.53	4.16

To further explore the influence of print direction on swelling percentage, the data was subjected to a Tukey-Kramer Honest Significant Difference (HSD) analysis ($p < 0.05$) using JMP 11 software (SAS Institute, Inc., Cary, NC, USA). This test is useful in increasing the confidence in the discernment of differences between sample sets beyond comparison based on standard deviation alone [41]. Results of this analysis are seen in Figures 3 and 4, and the significance is indicated by the color of the circle; when two circles are red, the sample pools are not significantly different, and when a circle is grey, that indicates a significant difference. While comparing the difference between PCL/TPU specimens exposed to acetic acid (Figure 3a), the mass loss for the 45° raster pattern specimens was found to be significantly different than the specimens fabricated in the 0° raster pattern, keeping in mind that the acetic acid leached material from the specimens. For PCL/TPU specimens exposed to ethyl acetate (Figure 3b) the amount of swelling for the 45° raster pattern specimens was significantly greater than the swelling exhibited for the specimens fabricated in the 0° raster pattern. This analysis reinforces the notion that there is a difference based on the raster pattern of the specimens in terms of swelling behavior.

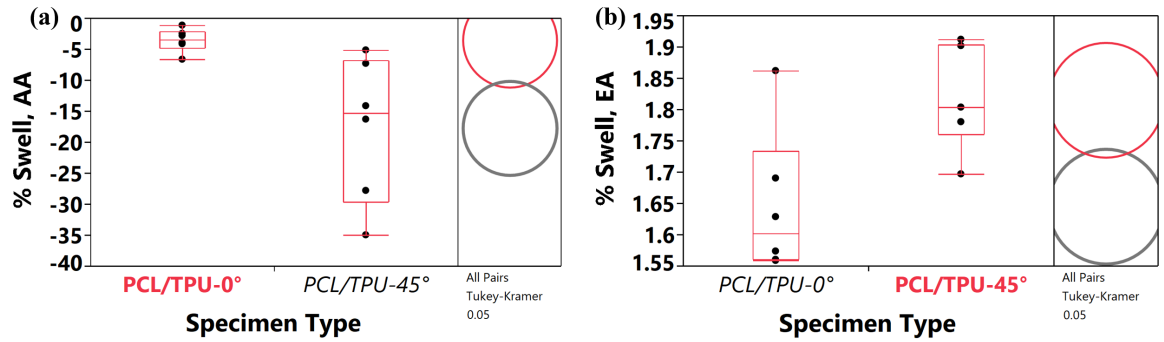

Figure 3. Tukey-Kramer HSD analysis of PCL/TPU specimens exposed to (**a**) acetic acid, and (**b**) ethyl acetate.

The data for the PCL/TPU/PLA blend specimens were also subjected to the Tukey-Kramer HSD test. The results are graphically represented in Figure 4. For PCL/TPU/PLA specimens exposed to acetic acid for 7 days (Figure 4a), the % swelling for the 45° raster pattern specimens was found to be significantly greater than those fabricated in a 0° raster pattern. However, the difference in swelling for specimens exposed to ethyl acetate (Figure 4b) was found to not be significantly different. This indicates that the ethyl acetate affects the ternary blend to a lesser extent than acetic acid.

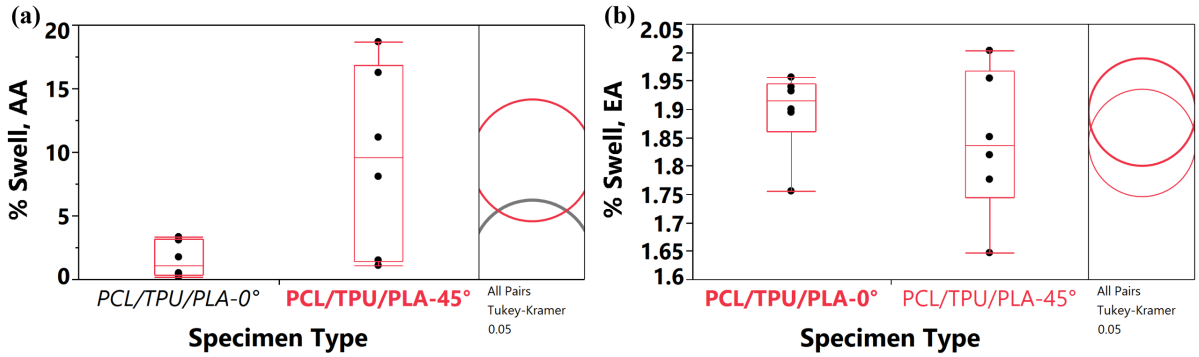

Figure 4. Tukey-Kramer HSD analysis of PCL/TPU/PLA of swelling data for specimens exposed to (**a**) acetic acid, and (**b**) ethyl acetate.

3.2. FTIR-ATR Analysis

The FTIR-ATR spectra for the ternary PCL/TPU/PLA blend after exposure to acetic acid and ethyl acetate are shown in Figure 5a,b, respectively. We have added some features to the spectra to make changes more discernible, where a dashed line indicates common peaks amongst all experimental groups, a red arrow indicates a peak that disappeared upon exposure to the organic substance, a green arrow and solid orange line indicates a peak that disappeared due to exposure to the organic substance and reappeared after thermal recovery, a white arrow on an orange solid line indicates a peak that changed intensity when experimental groups were compared, and a blue arrow indicates a peak that appeared due to exposure to the organic substance but disappeared due to the thermal recovery process. Comparing the control, exposed, and recovered specimens revealed significant changes after solvent exposure. The PCL/TPU/PLA sample exhibited absorbance in characteristic bands, mainly the carbonyl stretching from 1755 to 1735 cm^{-1} corresponding to ester groups present in PCL and PLA [42], peaks between 1180 to 1080 cm^{-1} characteristic of the C-O-C stretching group [43], and a N-H bending peak at 1530 cm^{-1} confirms the presence of the TPU urethane group [44], a peak at 3325 cm^{-1} is also visible.

The spectra for the specimens exposed to acetic acid exhibited a relative decrease in intensity of the C=O and C-O-C peaks, the O-H and N-H stretching peak at 3325 cm^{-1} disappears, and additional peaks at 1596 related to C-H vibrations [45] and 960 cm^{-1} attributed to C-O-C symmetric stretching [46,47], are strongly diminished, which indicates ester hydrolysis, interference of hydrogen-bonded urethane structures, and a reduction in crystalline PCL domains. The peak around 1530 cm^{-1} related to N-H groups [48], becomes less prominent when exposed to acetic acid and slightly clears after recovery. Equivalent decreases in the amide II, N-H peak have been attributed to urethane chain scission and changes in hard-segment restructuring [49], which support the interpretation that acetic acid interrupts the hydrogen-bonded urethane within the TPU segments.

Conversely, after exposure to ethyl acetate, an increase in the O-H band at 3325 cm^{-1} [50], indicating physical changes or reversible hydrogen bonding with a limited surface interaction. Related behavior has been reported in hydroxyl-containing polymers where increased O-H peak intensity close to 3325 cm^{-1} corresponds to improved or

restructured hydrogen bonding [51,52]. The carbonyl peak between 1720 to 1735 cm^{-1} attributed to carbonyl stretching vibrations [53] becomes more intense, indicating higher hydrogen bonding and dipolar interactions between the solvent and ester groups. This can be related to a previous study, which demonstrated carbonyl groups near 1720 cm^{-1} and an increase in intensity when the ester group forms hydrogen bonds with solvent molecules [54] The urethane N-H bending band at 1530 cm^{-1} and the CH_3 bending peak at 1450 cm^{-1} [55] increase in intensity. Some of these changes, involving the temporary disappearance of the crystalline PCL peak at 960 cm^{-1} [56], return to values similar to those of the control sample after recovery, demonstrating that ethyl acetate primarily stimulates reversible plasticization and swelling rather than permanent bond cleavage. Several peaks that disappear after acetic acid exposure reappear after ethyl acetate recovery, indicating acetic acid is more aggressive, producing irreversible chemical modifications, while ethyl acetate produces temporary and reversible interactions with the blend, which can be associated with a study that demonstrates PCL in acid solvent is chemically broken down and cannot recover it is original structure after treatment [57].

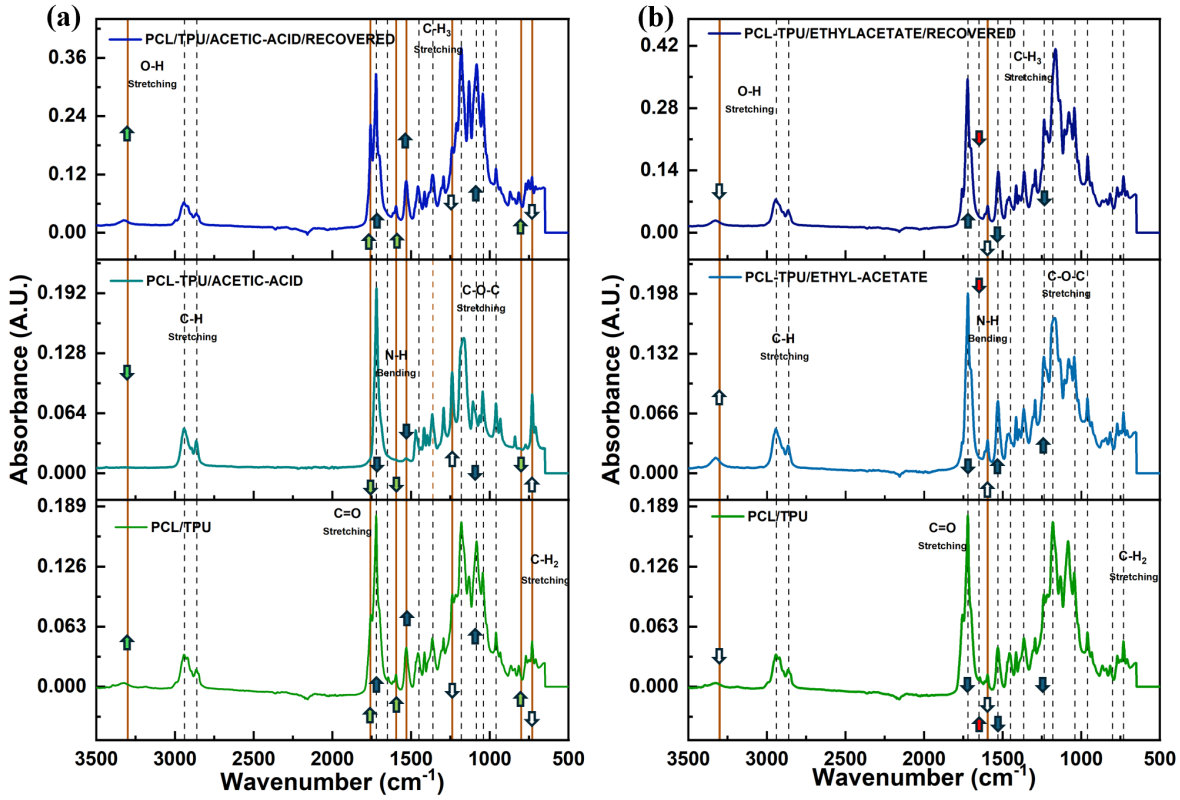

Figure 5. FTIR-ATR Spectra of the PCL/TPU/PLA blend for experiments involving (**a**) exposure to acetic acid and (**b**) exposure to ethyl acetate, where control specimens are compared to exposed specimens and specimens that were subjected to a thermal recovery cycle after exposure.

The FTIR-ATR spectra for PCL/TPU specimens are seen in Figure 6. for specimens exposed to acetic acid (Figure 6a) and ethyl acetate (Figure 6b). In comparison with the PCL/TPU/PLA, all the spectra exhibit less variation in C=O and O-H groups, due to the absence of PLA, which is susceptible to hydrolytic degradation [58]. In addition, the disappearance after acetic acid exposure of the O-H/N-H stretching signal at 3325 cm^{-1}, normally attributed to the urethane functional group [59,60] and hydroxyl groups [61], is observed. A peak related to crystalline PCL at 960 cm^{-1} [62,63] becomes strongly decreased. After recovery, ester-related peaks continue to attenuate, demonstrating permanent chemical modification due to hydrolytic cleavage of PCL segments, where ester bonds are irreversibly cleavage, forming carboxyl-terminated segments and minimizing the ester content of the material [64,65].

In comparison, ethyl acetate-exposed and recovered samples conserve similar carbonyl and ester peak intensities to the control sample, with a slight increase in the O-H peak, showing reversible solvent interaction without significant bond cleavage. The flexible nature of these changes denotes limited solvent penetration and non-destructive interaction with the polymer matrix. A dissimilar reaction was observed upon exposure to acetic acid, which induces hydrolytic degradation of the ester bond, ethyl acetate mainly promotes temporary plasticization through weak dipole and hydrogen bonding effects. Comparable solvent-polymer studies have demonstrated that the extent of chemical or

physical damage depends strongly on solvent polarity; alcohols such as ethanol and isopropanol promote irreversible chain disentanglement and dissolution in PMMA [66]. An absorption band typically appearing from 1520 to 1540 cm^{-1} is attributed to the NA N-H bending vibration of a secondary urethane group [67]. A N-H peak close to 1530 cm^{-1} becomes slightly prominent in both organic solvents, reflecting potential reorientation or interaction of TPU urethane segments with the solvent. However, because of acetic acid exposure, urethane N-H peaks at 1650 to 1580 cm^{-1} are significantly weakened or absent, demonstrating disruption of hydrogen-bonded urethane [68]. This statement aligns with the findings of Xu et al., who stated that acetic acid mainly interacts with oxygen and nitrogen-containing groups, leading to structural disruption and reduced molecular ordering [69]. A prominent C=O stretching band at 1735 cm^{-1} mainly from the ester groups in PCL [70], which decreases in intensity following exposure to acetic acid, indicating a potentially number of dipole interactions or potential ester bond hydrolysis at the surface. This is consistent with the surface erosion mechanism of PCL, in which hydrolytic chain scission occurs especially at the polymer interface rather than through the bulk [71,72].

FTIR results provide a molecular explanation for the difference in recovery and anisotropic mechanical performance visualized in FFF printed samples. Following attenuation of the C-O-C and C=O and crystalline PCL peaks after acetic acid exposure, reflecting degradation of polyester segments, minimizing chain mobility and weakens interfacial adhesion between PCL and TPU.

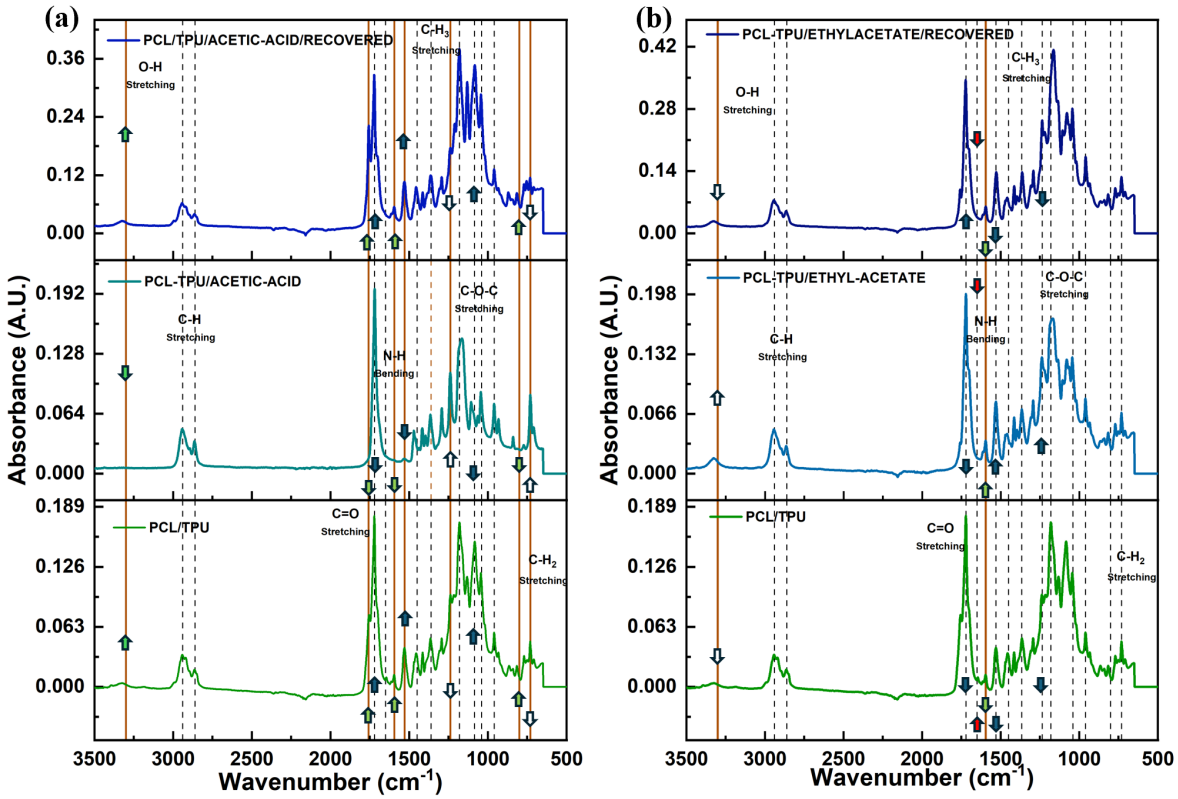

Figure 6. FTIR- ATR Spectra of the PCL/TPU blend for experiments involving (**a**) exposure to acetic acid and (**b**) exposure to ethyl acetate, where control specimens are compared to exposed specimens and specimens that were subjected to a thermal recovery cycle after exposure.

To determine the composition of the residual material recovered from the acetic acid containers post-treatment, 0.282 g from the container used for PCL/TPU specimens printed in the 0° raster pattern and the 1.186 g recovered from the container used for exposing the PCL/TPU specimens printed in the 45° were analyzed with FTIR-ATR. The resultant spectra are presented in Figure 7. Comparing the spectrum obtained from the residual specimens with that of pure PCL, reveals characteristic PCL absorption bands exhibiting C-H stretching vibrations around 2940 to 2960 cm^{-1}, a sharp C=O stretching peak at 1720 cm^{-1}, and noticeable C-O-C stretching vibrations between 1180 to 1040 cm^{-1}. The residual samples demonstrate a reduction in peak intensity, particularly for the C=O and C-O-C bands, signifying partial leaching degradation of ester bonds during the solvent exposure. Comparison of the spectra confirms that the residual material is composed of PCL. Moreover, the greater mass recovered from the 45° raster pattern container indicates that this raster pattern was more susceptible to exposure to acetic acid and agrees with the swell test data.

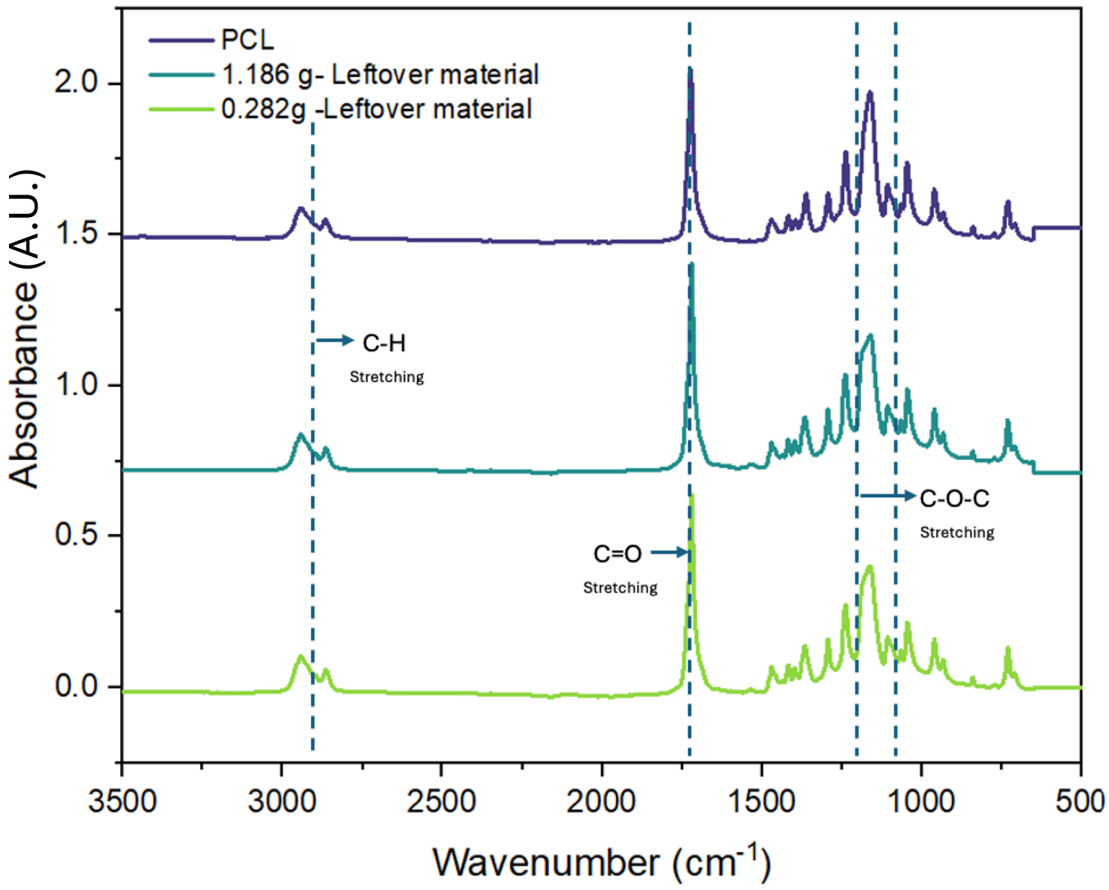

Figure 7. FTIR-ATR spectra of residuals recovered from the containers used for chemical exposure compared to PCL.

3.3. Tensile Testing

The tensile test results for specimens exposed to acetic acid are seen in Figure 8. In all cases, exposure to acetic acid lowered the UTS values as compared to control specimens for a given blend/raster pattern combination. As the goal of this work is to explicate the ability of self-healing mechanism induced by thermal annealing to recover from damage induced by chemical exposure, attention is given to differences in specimens annealed after exposure as compared to control specimens. The only sample pool to not demonstrate a level of recovery of strength after exposure to acetic acid was the PCL/TPU/PLA specimen fabricated in the 45° raster pattern. The control specimens for this sample pool yielded UTS values of 36.53 ± 8.16 MPa compared to 14.80 ± 14.47 MPa for specimens that were exposed to acetic acid. However, specimens that were annealed after exposure yielded UTS values of 7.60 ± 3.99 MPa, so no improvement was realized. We remind the reader that this sample pool also exhibited the greatest % swelling values. Conversely, the PCL/TPU/PLA specimens fabricated in a 0° raster pattern showed improvement in UTS values after annealing. The control specimens yielded a UTS value of 31.30 ± 7.20 MPa, while the exposed specimens yielded a UTS value of 10.57 ± 3.10 MPa. The annealed specimens showed an improvement in UTS, yielding a value of 20.33 ± 2.49 MPa. A noteworthy result was the improvement in UTS values for PCL/TPU printed in both raster patterns, given the mass loss of the specimens exposed to acetic acid. The annealed specimens fabricated in the 0° raster pattern showed an improvement in average UTS values as compared to the control sample pool (25.37 ± 0.67 MPa and 23.33 ± 7.42 MPa, respectively) though the difference is within error.

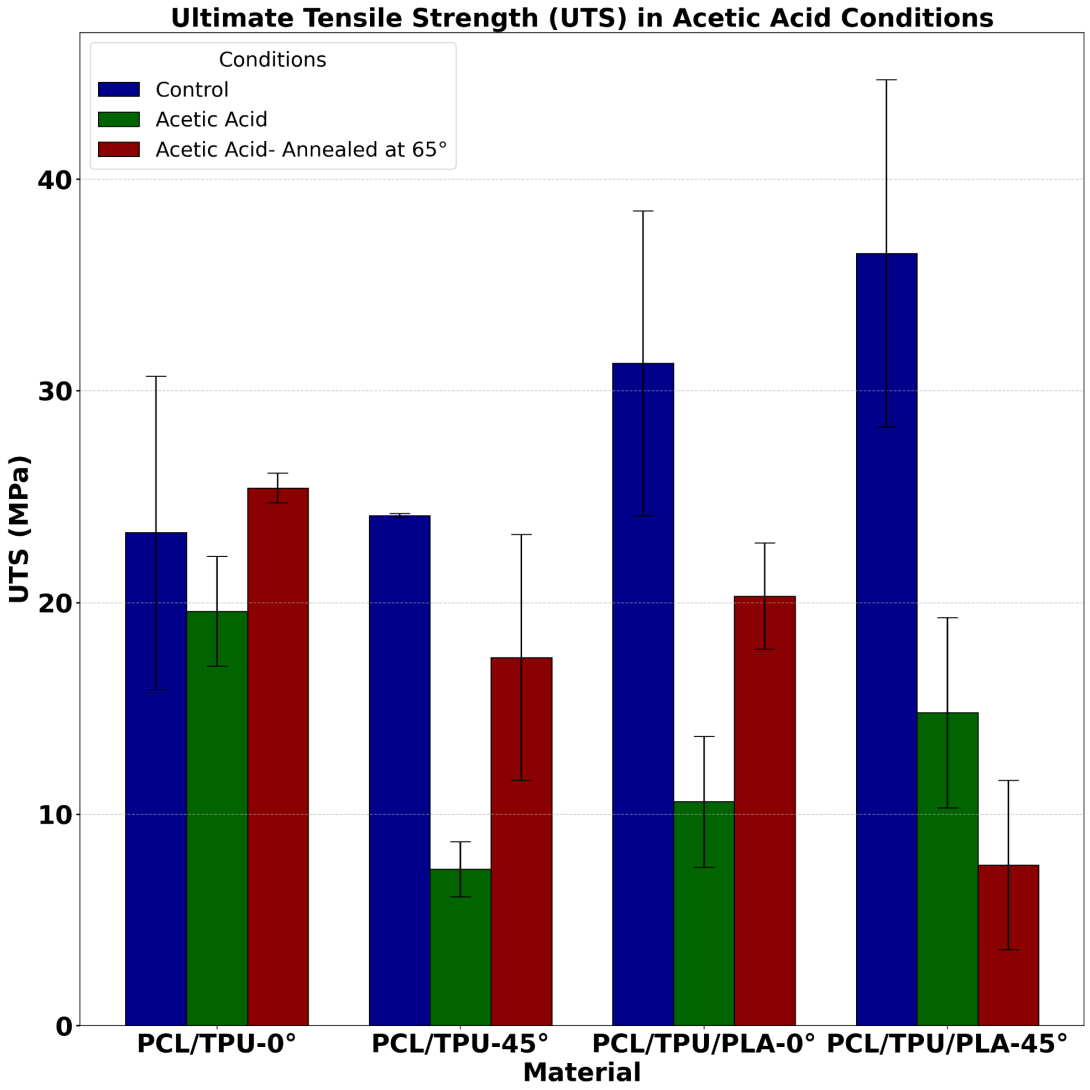

Figure 8. Ultimate Tensile Strength results of PCL/TPU and PCL/TPU/PLA for control specimens, specimens that were exposed to acetic acid, and specimens that were annealed after acetic acid exposure.

Exposure to ethyl acetate yielded a more complex mechanical response as seen in Figure 9. Most obvious is the increase in strength for PCL/TPU specimens printed in a 0° raster pattern which showed an unexpected increase in tensile strength after chemical exposure. The UTS value for the exposed specimens was 35.20 ± 5.28 MPa compared to the control values of 23.33 ± 7.42 MPa. Though unexpected, the result is within error. The PCL/TPU specimens fabricated in the 45° raster pattern also exhibited an increase in strength, though to a lesser degree, with UTS values of 25.67 ± 2.44 MPa compared to values of 24.10 ± 0.10 MPa, again, a result within the error. Annealing specimens composed of the PLA/TPU blend did not lead to an improvement in mechanical properties after exposure to ethyl acetate. On the other hand, specimens fabricated from the ternary PCL/TPU/PLA blend did exhibit an improvement in strength when comparing the data from specimens that were exposed to specimens that were annealed after exposure. UTS results of the materials tested here are tabularized in Table 3.

To evaluate the effectiveness of thermally activated self-healing mechanisms to mitigate damage incurred by chemical exposure, the tensile data was also subjected to Tukey-Kramer HSD analysis. In the case of PCL/TPU (Figure 10) the UTS values of 0° raster pattern specimens that were exposed to acetic acid and those that were annealed after exposure were found to not be significantly different than the control specimens (Figure 10a). However, for PCL/TPU specimens fabricated in the 45° raster pattern, exposure to acetic acid yielded UTS results significantly different than the control sample pool, and annealing led to UTS values that were not significantly different than the control specimens, meaning that annealing specimens first exposed to heated acetic acid for 7 days, mitigates damage incurred by exposure. Also, the print raster pattern plays a role in degree to which acetic acid damages additively manufactured PCL/TPU specimens.

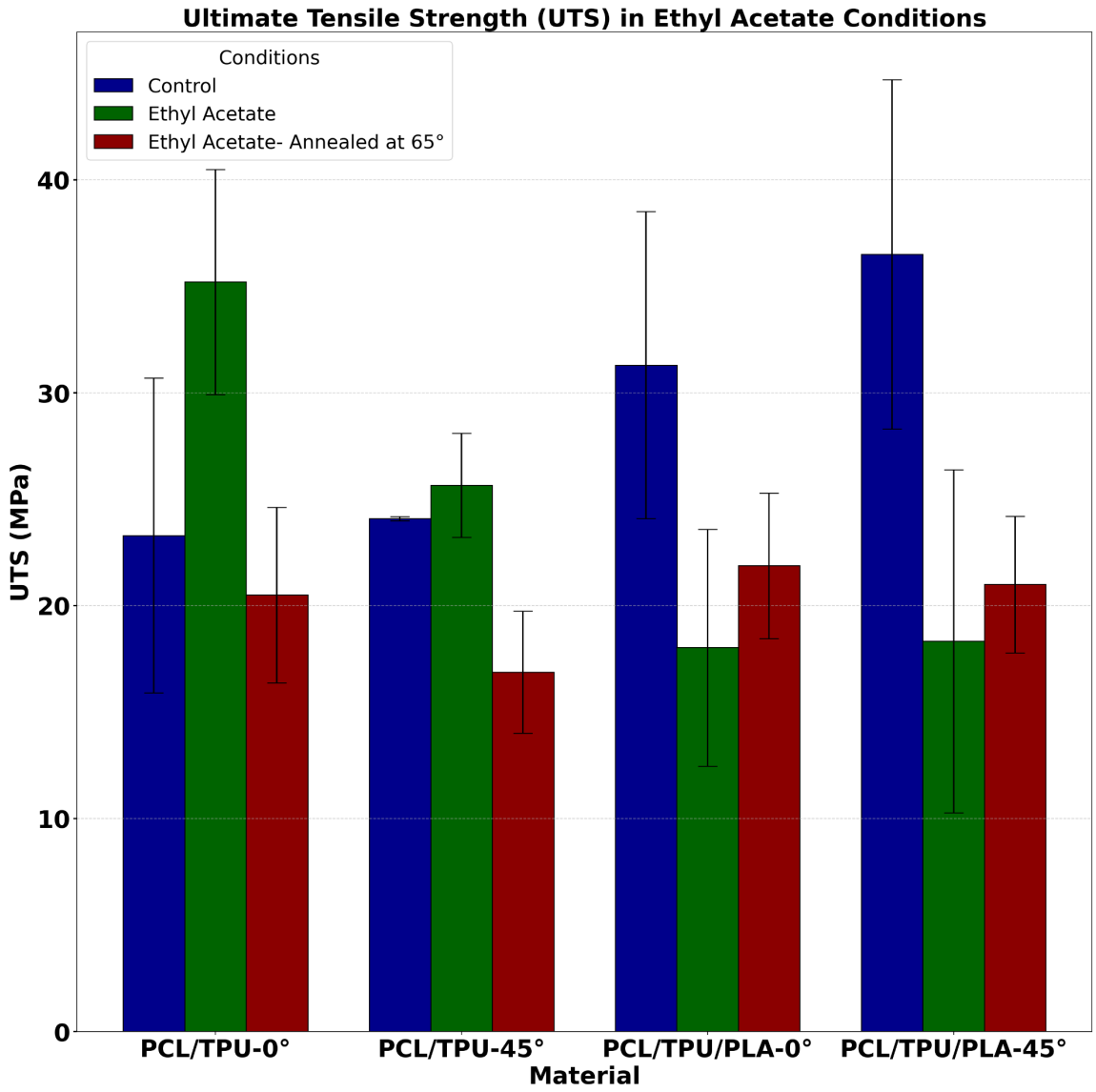

Figure 9. Ultimate Tensile Strength results of PCL/TPU and PCL/TPU/PLA for control specimens, specimens that were exposed to ethyl acetate, and specimens that were annealed after chemical exposure.

Table 3. UTS Results for this study.

	Control (MPa)	σ	Acetic Acid				Ethyl Acetate			
			Exposed (MPa)	σ	Annealed (MPa)	σ	Exposed (MPa)	σ	Annealed (MPa)	σ
PCL/TPU/PLA 0°	31.30	7.20	10.57	3.10	20.33	2.49	18.03	5.57	21.87	3.43
PCL/TPU/PLA 45°	36.53	8.16	14.80	4.47	7.60	3.99	18.33	8.06	21.00	3.22
PCL/TPU 0°	23.33	7.42	19.63	2.57	25.37	0.67	35.20	5.28	20.50	4.13
PCL/TPU 45°	24.10	0.10	7.37	1.30	17.43	5.79	25.67	2.44	16.87	2.86

Ethyl acetate interacted differently with the PCL/TPU specimens as compared to the specimens that were exposed to acetic acid. As mentioned previously, specimens fabricated in the 0° raster pattern exhibited an increase in strength after exposure to ethyl acetate, however this increase in strength was not found to be significantly different as seen in Figure 10c. The annealed 0° sample pool exhibited a decrease in strength, however, again, this was not found to be significantly different as compared to the control and exposed sample pools. When evaluating the results of the PCL/TPU specimens fabricated in a 45° raster pattern, a different behavior as compared to the 0° specimens is again observed. The UTS values of exposed specimens were found to be significantly different than the control specimen pools, while the annealed specimens exhibited an increase in strength making them statistically the same as the control specimen pool.

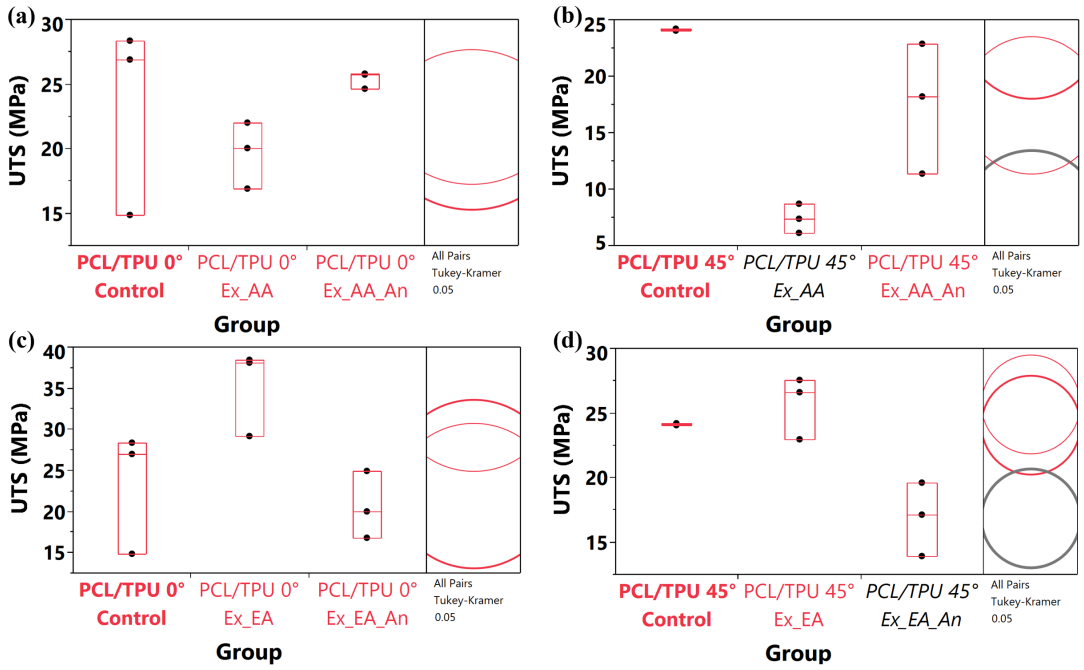

Figure 10. Tukey-Kramer HSD analysis for PCL/TPU specimens (**a**) printed in the 0° raster pattern and exposed to acetic acid, (**b**) printed in the 45° raster pattern and exposed to acetic acid, (**c**) printed in the 0° raster pattern and exposed to ethyl acetate, (**d**) printed in the 45° raster pattern and exposed ethyl acetate.

The Tukey-Kramer HSD analysis for PCL/TPU/PLA specimens is seen in Figure 11. For PCL/TPU/PLA specimens fabricated in the 0° raster pattern and exposed to acetic acid (Figure 11a) the UTS of the exposed specimens was significantly lower than the control specimens and the UTS values for the annealed specimens were statistically the same as the control specimens, indicating that annealing led to a mitigation of the damage induced by chemical exposure. However, for specimens fabricated in the 45° raster pattern (Figure 11b), annealing did not lead to a recovery of strength, as specimens that were exposed to acetic acid were statistically the same as those that were annealed after exposure, yet both were significantly lower as compared to the control sample pool. The distance of the circles for the 45° raster pattern indicates that the decrease in strength due to exposure is more significant than other experiments in this study meaning that there may be a point of no return in terms of the amount of damage sustained due to chemical exposure.

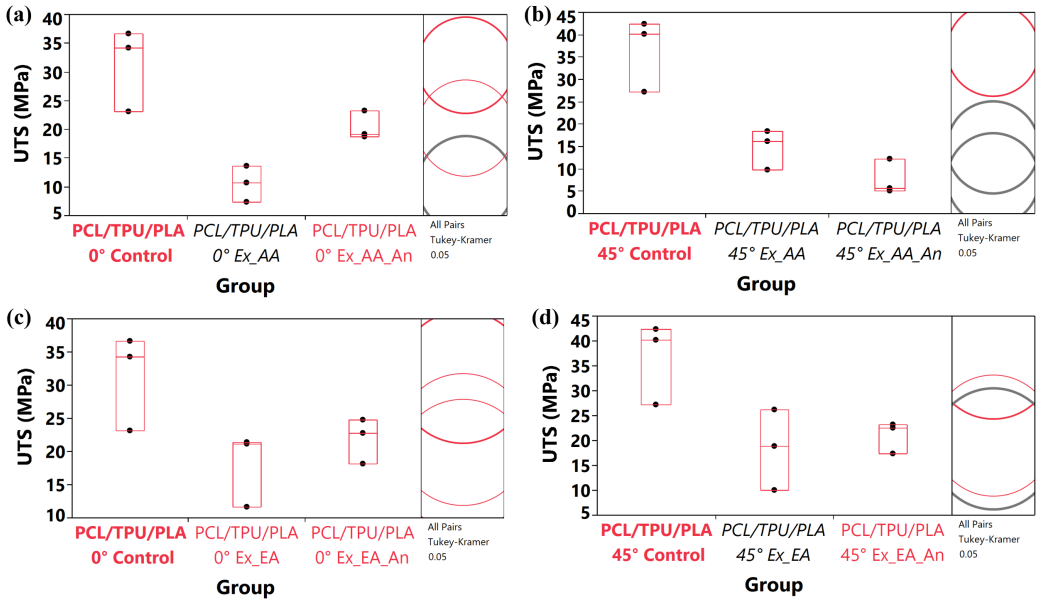

Figure 11. Tukey-Kramer HSD analysis for PCL/TPU/PLA specimens (**a**) printed in the 0° raster pattern and exposed to acetic acid, (**b**) printed in the 45° raster pattern and exposed to acetic acid, (**c**) printed in the 0° raster pattern and exposed to ethyl acetate, (**d**) printed in the 45° raster pattern and exposed ethyl acetate.

Specimens fabricated from PCL/TPU/PLA exposed to ethyl acetate behaved differently as compared to those exposed to acetic acid (Figure 11c,d). Though, in the case of 0° raster pattern specimens, exposure to acetic acid led to a decrease in UTS values (Figure 11c), while specimens that were annealed after exposure exhibited an increase in strength, both sample pools were not found to be honestly significantly different than the control sample pool. Somewhat conversely, the specimens fabricated in the 45° raster pattern and exposed to ethyl acetate (Figure 11d) yielded UTS values that were honestly significantly lower than the control sample pool while specimens that were annealed after chemical exposure yielded UTS values that were not significantly different than the control sample pool and honestly significantly greater than specimens that were exposed. Again, this indicates that the annealing process can mitigate damage induced by chemical exposure.

3.4. Scanning Electron Microscopy

To understand the effect of chemical exposure failure modes, the fracture surface of tensile test specimens was analyzed by SEM. For brevity we have only included images from the PCL/TPU specimens fabricated in the 0° raster pattern (Figure 12) and PCL/TPU/PLA specimens fabricated in the 45° raster pattern (Figure 13). In the case of PCL/TPU, the high elastomer content lends itself to a high amount of plastic deformation. The SEM micrograph of control specimen (Figure 12a) captures the side and the final rupture zone of the tensile specimen. The final rupture zone appears planar in nature, a feature driven by the reduction of area during the necking process that occurred during the tensile test. In the micrograph corresponding with the specimen that was exposed to acetic acid (Figure 12b), the material was more plasticized to the point that fibrils manifested on the ends of the failure zone (indicated by white dashed arrows). Delamination began to occur (pointed out by the solid white arrow) potentially meaning that the acetic acid attacked the interface between print rasters. Prior work involving exposing polyester specimens to liquid media [73] has characterized unique fracture surface features due to localized attack at the print raster interface so it is logical to assume similar mechanisms are occurring in this context as well. The specimen that was thermally recovered after ethyl acetate exposure (Figure 12c) sustained more plastic deformation prior to failure. We remind the reader that the recovered specimens for the 0° raster pattern exhibited greater UTS values than the specimens that were exposed to acetic acid with no thermal recovery cycle. The strengthening effect may be due to reflow of the PCL phase as the recovery temperature of 65° is in the range of the melting temperature of this material [74].

Exposure to ethyl acetate also led to an increase in UTS values and the fracture surface (Figure 12d) corresponds to this observation as the specimen failed on two planes along with a large amount of plastic deformation. Ethyl acetate is an effective solvent for TPU [75] and known to be added to TPU in the creation of urethane-based adhesives. We believe the addition of ethyl acetate effectively glued the print raster layers together, increasing strength. To that end, we believe the recovery process baked the solvent out weakening the material as indicated by the UTS values and the delamination between print rasters observed in the form of sheets which is seen in Figure 12e, and the higher magnification image in Figure 12f. The sheet morphology may be indicative of partial dissolution. The fracture surface morphology when taken in conjunction with the increase in O-H and N-H bonds for the specimens exposed to ethyl acetate, a chemical bond-driven strengthening and weaking process can be postulated.

The SEM micrographs in Figure 13 are from specimens composed of the PCL/TPU/PLA fabricated in the 45° raster pattern. The relatively lower elastomer content as compared to the binary blend (33.33% by mass as compared to 50% by mass) led to an expected lower amount of plastic deformation as was observed in Figure 13a. There is evidence of polymer diffusion between print raster beads, evident by an absence of the ability to discern the individual print raster beads particularly in the middle of the fracture surface, meaning that the print parameters used to fabricate the specimen were optimal [76–80]. Exposure to acetic acid (Figure 13b) led to a different fracture surface morphology where it is evident that more plastic deformation occurred corresponding with a ductile failure mechanism indicated by the presence of fibrils [81]. The fibrils are seen in greater detail in Figure 13c and indicated by dashed white arrows. The specimen exposed to acetic acid and then subjected to a thermal recovery cycle underwent more plastic deformation than the control specimen as indicated by the relatively smaller cross-sectional area consistent with more necking of the specimen. There is more plastic deformation on the fracture surface, but no delamination is observed. Though the specimen retained a near-square morphology when it failed, this sample pool did not realize an increase in UTS values.

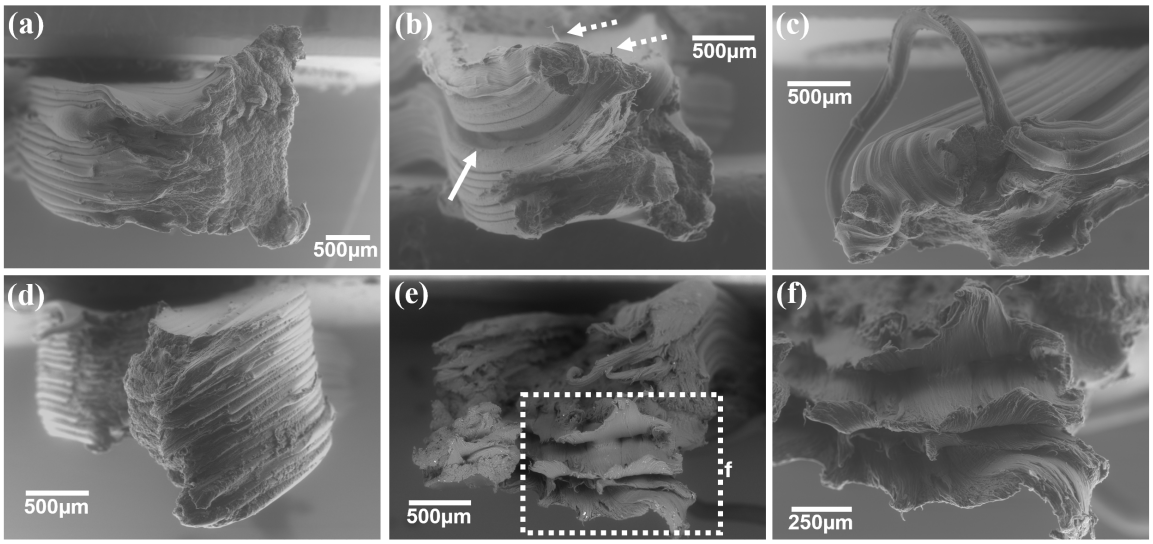

Figure 12. SEM micrographs of tensile specimen fracture surfaces fabricated from PCL/TPU in a 0° raster pattern where (**a**) is from a representative specimen from the control sample pool, (**b**) is a representative specimen from a specimen that was exposed to acetic acid, (**c**) is from a specimen that was exposed to acetic acid and then subjected to a thermal recovery cycle, (**d**) is from a specimen that was exposed to ethyl acetate, (**e**) is from a specimen that was exposed to ethyl acetate and then subjected to a thermal recovery cycle. The white dashed box in (**e**) corresponds to the image in (**f**).

Exposure of PCL/TPU/PLA specimens to ethyl acetate (Figure 13e) severely plasticized the material and the fracture surface of the tensile specimen also exhibited a large amount of plastic deformation with fibrils manifesting at the end of the specimen (highlighted by the white dashed arrow). Delamination of the specimen also occurred (highlighted by the solid white arrow) again indicating preferential inter-raster attack. The fracture surface of the recovered specimen (Figure 13f) also underwent a greater amount of plastic deformation as compared to the control specimen, however this sample pool yielded UTS values that were greater than the specimens that were exposed to ethyl acetate. The relatively lower content of TPU as compared to the binary blend seemingly negated any strengthening effect due to an interaction with ethyl acetate. We believe the strengthening effect due to the recovery cycle again to be attributed to the reflow of the PCL phase.

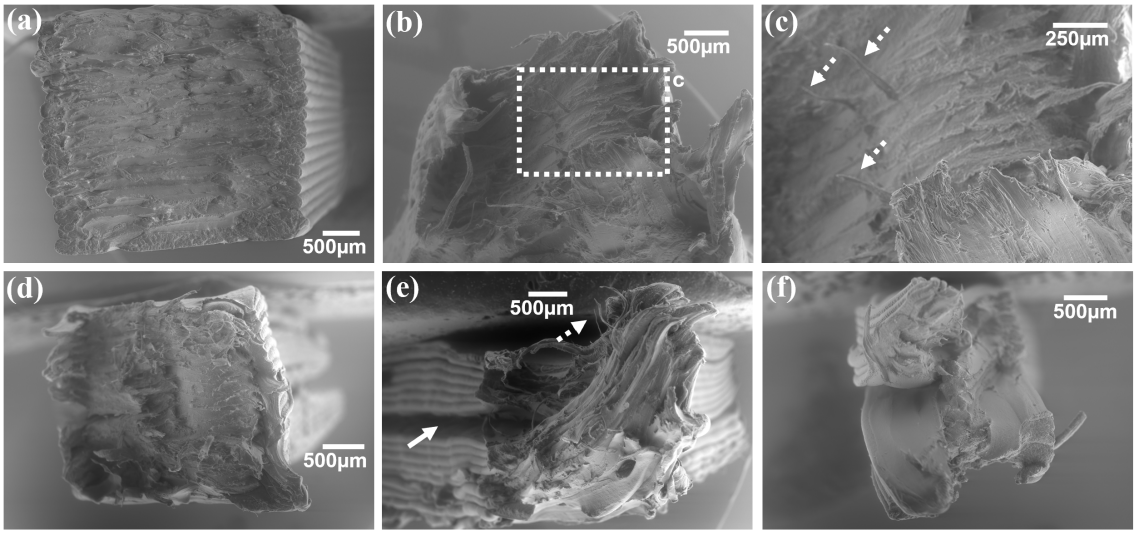

Figure 13. Fractographs of tensile specimens fabricated from PCL/TPU/PLA in a 45° raster pattern where (**a**) is from a representative specimen from the control sample pool, (**b**) is a specimen hat was exposed to acetic acid, (**c**) is a higher magnification image corresponding with the dashed box in (**b**), (**d**) is from a specimen that was subjected to a thermal revery cycle after exposure to acetic acid, (**e**) is from a specimen that was exposed to ethyl acetate, and (**f**) is from a specimen that was subjected to a thermal recovery cycle after exposure to ethyl acetate.

3.5. DMA

DMA specimens that were exposed to acetic acid were rendered too damaged to run in the instrumentation. The damage was characterized by delamination and severe warping of the specimen and an example is presented in Figure 14. The delamination of the print layers agrees with the conclusions drawn from the SEM microanalysis and again indicates preferential attack at the inter raster interface. As such we can only report the effect of ethyl acetate exposure in terms of DMA analysis**.**

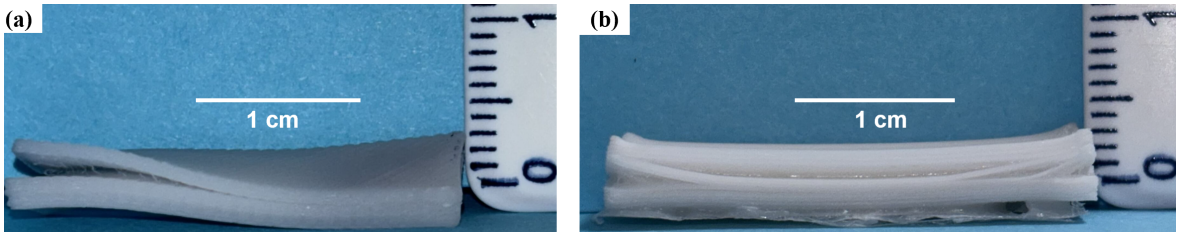

Figure 14. Examples of the damage caused by acetic acid exposure: (**a**) a PCL/TPU specimen fabricated in the 45° raster pattern and (**b**) a PCL/TPU/PLA specimen fabricated in a 0° raster pattern.

Exposure to ethyl acetate led to a decrease of the max tan δ, the ability of the material to dampen or dissipate energy as heat. As can be seen in Figure 15, both the PCL/TPU and PCL/TPU/PLA blends exhibited similar behavior at lower temperatures. However, once the temperature reached 50 °C, the effect of chemical exposure is observable. A somewhat surprising result was that the temperature at which the maximum temperature tan δ occurs was not affected by exposure to ethyl acetate, indicating that there was no effect on glass transition temperature, where it would be expected that this temperature would shift to a lower value. Annealing a PCL/TPU specimen after chemical exposure increased the max tan δ value, but not to the level of the control specimen. Signifying that the bulk polymer matrix was not meaningfully plasticized and that the solvent-induced damage occurred mostly at interfacial regions. Annealing a PCL/TPU/PLA also led to an increase in viscous response as indicated by a larger max tan δ value, as compared to the specimen exposed to ethyl acetate, but again, not to the level of the control specimen, and the level of increase was less than that observed for the PCL/TPU specimen.

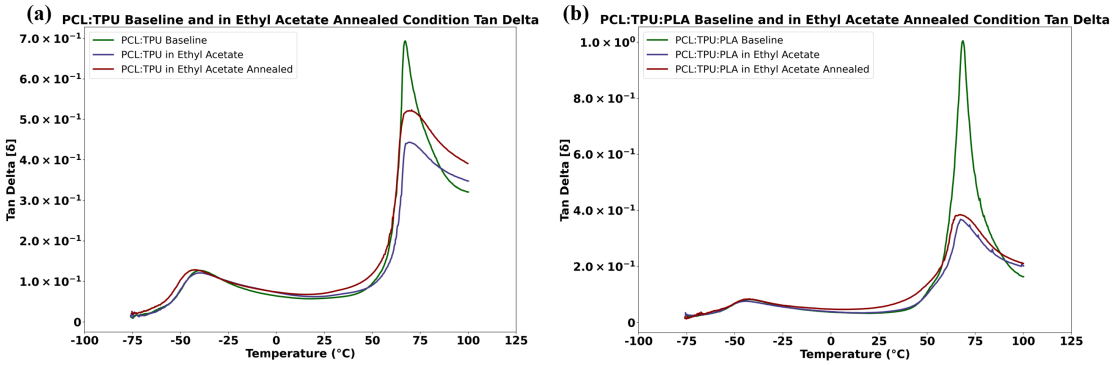

Figure 15. DMA results comparing baseline specimens with specimens exposed to ethyl acetate and specimens annealed after exposure to ethyl acetate for (**a**) PCL/TPU and (**b**) PCL/TPU/PLA for specimens fabricated in the 0° raster pattern.

4. Conclusions

Exposure to heated acetic acid or ethyl acetate induced damage to additively manufactured specimens composed of either a binary polymer blend made from an equal part by mass mixture of PCL and TPU blend or a ternary polymer blend made from equal parts of PCL, TPU, and PLA. The effect of this damage could be measured in terms of UTS. The severity of the damage varied based blend composition, the chemical the specimens were exposed to, and FFF print raster pattern. Heating of the acetic acid effectively created a harsh thermochemical environment leading to a large amount of damage to be sustained by the specimens. In some cases, namely PCL/TPU exposed to ethyl acetate, chemical exposure led to a slight increase in strength as compared to control sample pools for specimens fabricated in both the 0° and 45° raster patterns, though the difference was not found to be significant when the data was subjected to Tukey-Kramer HSD test.

As both of these materials are known to possess robust shape memory properties and annealing has been found to induce crystalline domains, increasing strength [21], it was proposed that applying the same thermal recovery cycle used to recover specimens during a shape memory test could be used to mitigate damage induced by chemical and thermochemical exposure. The results of this work do show that there is the potential for mitigating damage associated with chemical exposure though the application of a thermal annealing schedule after chemical exposure. In some cases, namely PCL/TPU exposed to acetic acid and fabricated in the 45° raster pattern, PCL/TPU/PLA fabricated in a 0° print raster pattern and exposed to acetic acid, and PCL/TPU/PLA fabricated in a 45° raster pattern and exposed to ethyl acetate, the strength was recovered to a point that it was found to be statistically the same as the control specimen pool. This was a significant finding because samples that were subject to chemical exposure with no annealing schedule yielded UTS values that were significantly lower than the control sample pool as verified by Tukey-Kramer HSD analysis.

Swell testing revealed that exposure to acetic acid caused mass loss for PCL/TPU specimens. The mass loss was significantly greater for specimens fabricated in the 45° raster pattern, indicating the ability of print raster to affect the uptake of chemicals for objects fabricated by FFF. FTIR-ATR analysis confirmed that acetic acid caused both reversible and irreversible chemical degradation in PCL/TPU and PCL/TPU/PLA blends, corroborated by the attenuation of ester-related C=O and C-O-C and the appearance of extensive O-H peaks due to the solvent treatments. The increase in N-H absorption demonstrates that TPU segments were also affected through new hydrogen-bonding interactions. In comparison, ethyl acetate exposure produces fewer and spectral changes, with the recovered sample showing peak intensities like the controls, validating that the ethyl acetate mainly induced physical swelling without breaking chemical bonds. The lesser degree of chemical degradation for ethyl acetate-exposed specimens was also most-likely due to the lack of applied heat. Microanalysis of the fracture surfaces of spent tensile test specimens via SEM revealed preferential attack of the inter-raster interface of the additively manufactured specimens for both the binary and ternary blends exposed to either ethyl acetate or acetic acid. Further evidence that acetic acid more severely damaged both blends was the fact that the DMA specimens were damaged to the degree that they could not be analyzed in our instrumentation.

Specimens exposed to ethyl acetate were able to be analyzed by DMA. Analysis revealed that exposure to ethyl acetate led to a decrease in max tan δ, but not the temperature at which this property was reached. Annealing specimens increased the max tan δ, but not to the level of control specimens in the case of PCL/TPU. In the case of PCL/TPU/PLA, the increase in max tan δ was also observed, but to a lesser degree.

Though the damage to specimens was present, the ability to recover the mechanical properties of a component damaged by chemical exposure has been demonstrated. A facile thermal annealing process could potentially render polymeric components fabricated from materials with known shape memory/self-healing properties recoverable, thereby increasing component life and reducing the generation of polymeric waste by removing the need to discard a damaged component and replace it with a new one.

Author Contributions

Conceptualization, D.A.R. and K.L.D.R.; methodology, D.A.R. and K.L.D.R.; validation, D.A.R., K.L.D.R. and S.M.; formal analysis, K.L.D.R., S.M. and O.B.; investigation, D.A.R., S.M., O.B. and K.L.D.R.; resources, D.A.R.; data curation, D.A.R., K.L.D.R, S.M. and O.B..; writing—original draft preparation, K.L.D.R, D.A.R., S.M. and O.B.; writing—review and editing, D.A.R., O.B., S.M. and K.L.D.R.; supervision, D.A.R.; project administration, D.A.R.; funding acquisition, D.A.R. All authors have read and agreed to the published version of the manuscript.

Funding

This research was funded by the National Science Foundation (NSF) under grant number CMMI 2227573. The APC was funded by the same agency and grant.

Data Availability Statement

The data supporting the findings of this study are available from the corresponding author upon reasonable request.

Acknowledgments

The work presented here was performed in the Polymer Extrusion Lab in the Department of Metallurgical, Materials, and Biomedical Engineering (MMBME) at The University of Texas at El Paso (UTEP). The authors also acknowledge support from the Mr. and Mrs. Macintosh Murchison Chair III in Engineering.

Conflicts of Interest

The authors declare no conflicts of interest.

Use of AI and AI-Assisted Technologies

No AI tools were utilized for this paper.

References

1. Akhbarizadeh, R.; Moore, F.; Keshavarzi, B. Investigating Microplastics Bioaccumulation and Biomagnification in Seafood from the Persian Gulf: A Threat to Human Health? *Food Addit. Contam. Part A* **2019**, *36*, 1696–1708.
2. Smith, M.; Love, D.C.; Rochman, C.M.; et al. Microplastics in Seafood and the Implications for Human Health. *Food Health Environ.* **2018**, *5*, 375–386.
3. Jenner, L.C.; Rotchell, J.M.; Bennett, R.T.; et al. Detection of Microplastics in Human Lung Tissue Using μFTIR Spectroscopy. *Sci. Total Environ.* **2022**, *831*, 154907. https://doi.org/10.1016/j.scitotenv.2022.154907.
4. Ragusa, A.; Svelato, A.; Santacroce, C.; et al. Plasticenta: First Evidence of Microplastics in Human Placenta. *Environ. Int.* **2021**, *146*, 106274. https://doi.org/10.1016/j.envint.2020.106274.
5. Schwabl, P.; Köppel, S.; Dipl-Ing, K.; et al. Detection of Various Microplastics in Human Stool. *Ann. Intern. Med.* **2019**, *171*, 453–457.
6. Zhang, N.; Li, Y.B.; He, H.R.; et al. You Are What You Eat: Microplastics in the Feces of Young Men Living in Beijing. *Sci. Total Environ.* **2021**, *767*, 144345. https://doi.org/10.1016/j.scitotenv.2020.144345.
7. Cox, K.D.; Covernton, G.A.; Davies, H.L.; et al. Human Consumption of Microplastics. *Environ. Sci. Technol.* **2019**, *53*, 7068–7074.
8. Cavender-Word, T.J.; Roberson, D.A. Development of a Resilience Parameter for 3D-Printable Shape Memory Polymer Blends. *Materials* **2023**, *16*, 5906. https://doi.org/10.3390/ma16175906.
9. Hornat, C.C.; Urban, M.W. Shape Memory Effects in Self-Healing Polymers. *Prog. Polym. Sci.* **2020**, *102*, 101208. https://doi.org/10.1016/j.progpolymsci.2020.101208.
10. Self-Healing Polymers|Nature Reviews Materials. Available online: https://www.nature.com/articles/s41578-020-0202-4 (accessed on 11 November 2025).
11. Zhang, W.; Chen, L.; Zhang, Y. Surprising Shape-Memory Effect of Polylactide Resulted from Toughening by Polyamide Elastomer. *Polymer* **2009**, *50*, 1311–1315. https://doi.org/10.1016/j.polymer.2009.01.032.
12. Quiñonez, P.A.; Bermudez, D.; Ugarte-Sanchez, L.; et al. Tailoring Physical Properties of Shape Memory Polymers for FDM-Type Additive Manufacturing. In Proceedings of the 30th Annual International Solid Freeform Fabrication Symposium—An Additive Manufacturing Conference, Austin, TX, USA, 12 August 2019; pp. 843–855.
13. Quiñonez, P.A.; Ugarte-Sanchez, L.; Bermudez, D.; et al. Design of Shape Memory Thermoplastic Material Systems for Fdm-Type Additive Manufacturing. *Materials* **2021**, *14*, 4254. https://doi.org/10.3390/ma14154254.
14. Lai, S.-M.; Lan, Y.-C. Shape Memory Properties of Melt-Blended Polylactic Acid (PLA)/Thermoplastic Polyurethane (TPU) Bio-Based Blends. *J. Polym. Res.* **2013**, *20*, 140. https://doi.org/10.1007/s10965-013-0140-6.
15. Rahmatabadi, D.; Soltanmohammadi, K.; Aberoumand, M.; et al. 4D Printing of Porous PLA-TPU Structures: Effect of Applied Deformation, Loading Mode and Infill Pattern on the Shape Memory Performance. *Phys. Scr.* **2024**, *99*, 025013. https://doi.org/10.1088/1402-4896/ad1957.
16. Shin, E.J.; Jung, Y.S.; Park, C.H.; et al. Eco-Friendly TPU/PLA Blends for Application as Shape-Memory 3D Printing Filaments. *J. Polym. Env.* **2023**, *31*, 3182–3196. https://doi.org/10.1007/s10924-023-02799-w.
17. Pinto, L.A.; Backes, E.H.; Harb, S.V.; et al. Shape Memory Thermoplastic Polyurethane/Polycaprolactone Blend and Composite with Hydroxyapatite for Biomedical Application. *J. Mater. Res.* **2024**, *39*, 90–106. https://doi.org/10.1557/s43578-023-01172-w.
18. Rahmatabadi, D.; Aberoumand, M.; Soltanmohammadi, K.; et al. 4D Printing-Encapsulated Polycaprolactone–Thermoplastic Polyurethane with High Shape Memory Performances. *Adv. Eng. Mater.* **2023**, *25*, 2201309. https://doi.org/10.1002/adem.202201309.
19. 4D Printing-Encapsulated Polycaprolactone–Thermoplastic Polyurethane with High Shape Memory Performances-Rahmatabadi-2023-Advanced Engineering Materials—Wiley Online Library. Available online: https://advanced.onlinelibrary.wiley.com/doi/full/10.1002/adem.202201309 (accessed on 1 July 2025).
20. Tunable Shape Memory Performances via Multilayer Assembly of Thermoplastic Polyurethane and Polycaprolactone|ACS Applied Materials & Interfaces. Available online: https://pubs.acs.org/doi/full/10.1021/acsami.5b10246?casa_token=FdGHzyQMtP8AAAAA%3Atq9iwy1WPh9H2GXjLxCyg37yajA0MOXsaASPgUrMm2tP3WSx2thEM8JefMnmJk6vihDV-dY6NVabU0c (accessed on 1 July 2025).

21. Carrillo, L.E.L.; Gonzalez, Y.O.; Parga, M.; et al. Development of Binary and Ternary Polyester Shape Memory Blends for Additive Manufacturing. *J. Mater. Sci.* **2024**, *59*, 8040–8057. https://doi.org/10.1007/s10853-024-09657-7.
22. Delgado Ramos, K.L.; Moreno, S.; Roberson, D.A. Fracture Surface Analysis, Mechanical Property Anisotropy, and Self-Healing Evaluation of Additively Manufactured Polyester Blends. *J. Fail. Anal. Preven.* **2025**, *25*, 1921–1936. https://doi.org/10.1007/s11668-025-02255-y.
23. Wool, R.P.; O'Connor, K.M. A Theory Crack Healing in Polymers. *J. Appl. Phys.* **1981**, *52*, 5953–5963. https://doi.org/10.1063/1.328526.
24. Peng, Y.; Gu, S.; Wu, Q.; et al. High-Performance Self-Healing Polymers. *Acc. Mater. Res.* **2023**, *4*, 323–333. https://doi.org/10.1021/accountsmr.2c00174.
25. Wang, S.; Urban, M.W. Self-Healing Polymers. *Nat. Rev. Mater.* **2020**, *5*, 562–583. https://doi.org/10.1038/s41578-020-0202-4.
26. Bhattacharya, S.; Hailstone, R.; Lewis, C.L. Thermoplastic Blend Exhibiting Shape Memory-Assisted Self-Healing Functionality. *ACS Appl. Mater. Interfaces* **2020**, *12*, 46733–46742. https://doi.org/10.1021/acsami.0c13645.
27. Jian, X.; Hu, Y.; Zhou, W.; et al. Self-Healing Polyurethane Based on Disulfide Bond and Hydrogen Bond. *Polym. Adv. Technol.* **2018**, *29*, 463–469. https://doi.org/10.1002/pat.4135.
28. Fu, Y.; Xu, F.; Weng, D.; et al. Superhydrophobic Foams with Chemical- and Mechanical-Damage-Healing Abilities Enabled by Self-Healing Polymers. *ACS Appl. Mater. Interfaces* **2019**, *11*, 37285–37294. https://doi.org/10.1021/acsami.9b11858.
29. Ferreira, J.L.; Gomes, S.; Henriques, C.; et al. Electrospinning Polycaprolactone Dissolved in Glacial Acetic Acid: Fiber Production, Nonwoven Characterization, and In Vitro Evaluation. *J. Appl. Polym. Sci.* **2014**, *131*. https://doi.org/10.1002/app.41068.
30. Zhang, X.; Espiritu, M.; Bilyk, A.; et al. Morphological Behaviour of Poly(Lactic Acid) during Hydrolytic Degradation. *Polym. Degrad. Stab.* **2008**, *93*, 1964–1970. https://doi.org/10.1016/j.polymdegradstab.2008.06.007.
31. Rossignolo, G.; Malucelli, G.; Lorenzetti, A. Recycling of Polyurethanes: Where We Are and Where We Are Going. *Green Chem.* **2024**, *26*, 1132–1152. https://doi.org/10.1039/D3GC02091F.
32. Gao, C.; Meng, L.; Yu, L.; et al. Preparation and Characterization of Uniaxial Poly(Lactic Acid)-Based Self-Reinforced Composites. *Compos. Sci. Technol.* **2015**, *117*, 392–397. https://doi.org/10.1016/j.compscitech.2015.07.006.
33. Theron, J.P.; Knoetze, J.H.; Sanderson, R.D.; et al. Modification, Crosslinking and Reactive Electrospinning of a Thermoplastic Medical Polyurethane for Vascular Graft Applications. *Acta Biomater.* **2010**, *6*, 2434–2447. https://doi.org/10.1016/j.actbio.2010.01.013.
34. Zhang, S.; Campagne, C.; Salaün, F. Preparation of Electrosprayed Poly(Caprolactone) Microparticles Based on Green Solvents and Related Investigations on the Effects of Solution Properties as Well as Operating Parameters. *Coatings* **2019**, *9*, 84. https://doi.org/10.3390/coatings9020084.
35. *D20.10 Subcommittee ASTM Standard D638*; Standard Test Method for Tensile Properties of Plastics 2022. ASTM International: West Conshohocken, PA, USA, 2022.
36. *E37.10 Subcommittee ASTM Standard E1640*; Standard Test Method for Assignment of the Glass Transition Temperature By Dynamic Mechanical Analysis. ASTM International: West Conshohocken, PA, USA, 2023.
37. Lares Carrillo, L.E.; Salazar, J.F.; Hitter, M.M.; et al. The Effect of Raster Pattern and Acetic Acid Exposure on the Mechanical and Failure Properties of Additively Manufactured PLA and PLA-Wood Composite Specimens. *J Fail. Anal. Preven.* **2023**, *23*, 1298–1312. https://doi.org/10.1007/s11668-023-01681-0.
38. Mahmud, M.S.; Delgadillo, A.; Urbay, J.E.M.; et al. Chemical Aging and Degradation of Stereolithographic 3D-Printed Material: Effect of Printing and Post-Curing Parameters. *Polym. Degrad. Stab.* **2025**, *232*, 111151. https://doi.org/10.1016/j.polymdegradstab.2024.111151.
39. Franklin, S. Effect of Different Heating Temperatures and Acetic Acid Concentrations on Physical Quality of Curd as an Ingredient for Milk Nuggets. Available online: https://researcherslinks.com/current-issues/Effect-of-Different-Heating-Temperatures/34/1/10521/html (accessed on 11 November 2025).
40. Kim, E.; Shin, Y.-J.; Ahn, S.-H. The Effects of Moisture and Temperature on the Mechanical Properties of Additive Manufacturing Components: Fused Deposition Modeling. *Rapid. Prototyp. J.* **2016**, *22*, 887–894. https://doi.org/10.1108/RPJ-08-2015-0095.
41. Lane, D.M. Tukey's Honestly Significant Difference (HSD). In *Encyclopedia of Research Design*; SAGE Publications, Inc.: Thousand Oaks, CA, USA, 2010; pp. 1566–1570. ISBN 978-1-4129-6128-8.
42. Bermudez, D.; Quiñonez, P.A.; Vasquez, E.J.; et al. A Comparison of the Physical Properties of Two Commercial 3D Printing PLA Grades. *Virtual Phys. Prototyp.* **2021**, *16*, 178–195. https://doi.org/10.1080/17452759.2021.1910047.
43. Sun, T.; Bian, J.; Wang, Y.; et al. One-Step Synthesis of Poly(L-Lactic Acid)-Based Soft Films with Gas Permselectivity for White Mushrooms (Agaricus Bisporus) Preservation. *Foods* **2023**, *12*, 586. https://doi.org/10.3390/foods12030586.

44. Nordi, S.S.; Noor, E.E.M.; Kok, C.K.; et al. Phase, Chemical, Thermal, and Morphological Analyses of Thermoplastic Polyurethane (TPU) Nanocomposites Reinforced with Jute Cellulose Nanofibers (CNFs). *Polymers* **2025**, *17*, 899. https://doi.org/10.3390/polym17070899.
45. Perin, D.; Dorigato, A.; Pegoretti, A. Thermoplastic Self-Healing Polymer Blends for Structural Composites: Development of Polyamide 6 and Cyclic Olefinic Copolymer Blends. *J. Appl. Polym. Sci.* **2023**, *140*, e53751. https://doi.org/10.1002/app.53751.
46. Verma, D.; Katti, K.; Katti, D. Experimental Investigation of Interfaces in Hydroxyapatite/Polyacrylic Acid/Polycaprolactone Composites Using Photoacoustic FTIR Spectroscopy. *J. Biomed. Mater. Res. Part A* **2006**, *77A*, 59–66. https://doi.org/10.1002/jbm.a.30592.
47. Ganbaatar, S.E.; Kim, H.-K.; Kang, N.-U.; et al. Calcium Phosphate (CaP) Composite Nanostructures on Polycaprolactone (PCL): Synergistic Effects on Antibacterial Activity and Osteoblast Behavior. *Polymers* **2025**, *17*, 200. https://doi.org/10.3390/polym17020200.
48. Olszewski, A.; Kosmela, P.; Piasecki, A.; et al. Comprehensive Investigation of Stoichiometry–Structure–Performance Relationships in Flexible Polyurethane Foams. *Polymers* **2022**, *14*, 3813. https://doi.org/10.3390/polym14183813.
49. Monteiro, W.F.; Miranda, G.M.; Soares, R.R.; et al. Weathering Resistance of Waterborne Polyurethane Coatings Reinforced with Silica from Rice Husk Ash. *An. Acad. Bras. Ciênc.* **2019**, *91*, e20181190. https://doi.org/10.1590/0001-3765201920181190.
50. Kim, S. Characterization of Mechanical, Thermal and Rheological Properties of Silica-Based Nanocomposite Filled Thermoplastic Polyurethane Film. *Macromol. Res.* **2024**, *32*, 727–743. https://doi.org/10.1007/s13233-024-00286-2.
51. Morita, S. Hydrogen-Bonds Structure in Poly(2-Hydroxyethyl Methacrylate) Studied by Temperature-Dependent Infrared Spectroscopy. *ResearchGate* **2025**, *2*, 10. https://doi.org/10.3389/fchem.2014.00010.
52. Smith, B.C. The Infrared Spectra of Polymers, VI: Polymers With C-O Bonds|Spectroscopy Online. Available online: https://www.spectroscopyonline.com/view/the-infrared-spectra-of-polymers-vi-polymers-with-c-o-bonds?utm_source=chatgpt.com (accessed on 13 November 2025).
53. Defeyt, C.; Langenbacher, J.; Rivenc, R. Polyurethane Coatings Used in Twentieth Century Outdoor Painted Sculptures. Part I: Comparative Study of Various Systems by Means of ATR-FTIR Spectroscopy. *Herit. Sci.* **2017**, *5*, 11. https://doi.org/10.1186/s40494-017-0124-7.
54. Dreier, L.B.; Bonn, M.; Backus, E.H.G. Hydration and Orientation of Carbonyl Groups in Oppositely Charged Lipid Monolayers on Water. *J. Phys. Chem. B* **2019**, *123*, 1085–1089. https://doi.org/10.1021/acs.jpcb.8b12297.
55. Hashim, Z.; Zaki, S.; Muhamad, I. Quality Assessment of Fried Palm Oils Using Fourier Transform Infrared Spectroscopy and Multivariate Approach. *Chem. Eng. Trans.* **2017**, *56*, 829–834. https://doi.org/10.3303/CET1756139.
56. Elzein, T.; Nasser-Eddine, M.; Delaite, C.; et al. FTIR Study of Polycaprolactone Chain Organization at Interfaces. *J. Colloid Interface Sci.* **2004**, *273*, 381–387. https://doi.org/10.1016/j.jcis.2004.02.001.
57. Anaya-Mancipe, J.M.; de Figueiredo, A.C.; Rabello, L.G.; et al. Evaluation of the Polycaprolactone Hydrolytic Degradation in Acid Solvent and Its Influence on the Electrospinning Process. *J. Appl. Polym. Sci.* **2024**, *141*, e55662. https://doi.org/10.1002/app.55662.
58. Siqueiros, J.G.; Roberson, D.A. In Situ Wire Drawing of Phosphate Glass in Polymer Matrices for Material Extrusion 3D Printing. *Int. J. Polym. Sci.* **2017**, *2017*, 1954903. https://doi.org/10.1155/2017/1954903.
59. Wang, Y.; Nie, H.; Wang, S.; et al. Dual-Functional Biopolyurethane Blends with Shape-Memory and Self-Healing Properties: Effects of Mixed Hard Domains on Structures and Properties. *ACS Appl. Polym. Mater.* **2023**, *5*, 9364–9374. https://doi.org/10.1021/acsapm.3c01865.
60. Petrović, Z.S.; Djonlagić, J.; Hong, J.; et al. Structure Development in Cross-Linked, Soybean Oil-Based Waterborne Polyurethanes. *J. Polym. Env.* **2025**, *33*, 2091–2108. https://doi.org/10.1007/s10924-024-03368-5.
61. Castro, J.I.; Araujo-Rodríguez, D.G.; Valencia-Llano, C.H.; et al. Biocompatibility Assessment of Polycaprolactone/Polylactic Acid/Zinc Oxide Nanoparticle Composites Under In Vivo Conditions for Biomedical Applications. *Pharmaceutics* **2023**, *15*, 2196. https://doi.org/10.3390/pharmaceutics15092196.
62. Archer, E.; Torretti, M.; Madbouly, S. Biodegradable Polycaprolactone (PCL) Based Polymer and Composites. *Phys. Sci. Rev.* **2023**, *8*, 4391–4414. https://doi.org/10.1515/psr-2020-0074.
63. Mohammed, K.S.; Coskun, M.; Babakr, K.A.; et al. Blending of Polycaprolactone with Polyvinyl Chloride Polymers Using Silica Gel as a Functional Reinforcement. *J. Mater. Sci. Mater. Electron.* **2025**, *36*, 2020. https://doi.org/10.1007/s10854-025-16102-1.
64. Salaris, V.; López, D.; Kenny, J.M.; et al. Hydrolytic Degradation and Bioactivity of Electrospun PCL-Mg-NPs Fibrous Mats. *Molecules* **2023**, *28*, 1001. https://doi.org/10.3390/molecules28031001.
65. Leroux, A.; Nguyen, T.N.; Rangel, A.; et al. Long-Term Hydrolytic Degradation Study of Polycaprolactone Films and Fibers Grafted with Poly(Sodium Styrene Sulfonate): Mechanism Study and Cell Response. *Biointerphases* **2020**, *15*, 061006. https://doi.org/10.1116/6.0000429.

66. Kavda, S.; Golfomitsou, S.; Richardson, E. Effects of Selected Solvents on PMMA after Prolonged Exposure: Unilateral NMR and ATR-FTIR Investigations. *Herit. Sci.* **2023**, *11*, 63. https://doi.org/10.1186/s40494-023-00881-z.
67. Smith, B.C. Organic Nitrogen Compounds IX: Urethanes and Diisocyanates|Spectroscopy Online. Available online: https://www.spectroscopyonline.com/view/organic-nitrogen-compounds-ix-urethanes-and-diisocyanates (accessed on 12 November 2025).
68. Djouadi, Z.; Vinogradoff, V.; Dionnet, Z.; et al. Asuka 12236 More Primitive than Paris: Clues given by Their Infrared and Raman Micro-Spectroscopy Signatures. *Meteorit. Planet. Sci.* **2025**, *60*, 1851–1860. https://doi.org/10.1111/maps.70017.
69. Zhang, H.; Mao, X.; Du, S.; et al. Micromechanism of the Effect of Coal Functional Groups on the Catalytic/Esterification Reaction of Acetic Acid. *J. Mol. Liq.* **2024**, *411*, 125796. https://doi.org/10.1016/j.molliq.2024.125796.
70. Nashchekina, Y.; Chabina, A.; Moskalyuk, O.; et al. Effect of Functionalization of the Polycaprolactone Film Surface on the Mechanical and Biological Properties of the Film Itself. *Polymers* **2022**, *14*, 4654. https://doi.org/10.3390/polym14214654.
71. Kayan, G.Ö.; Kayan, A. Polycaprolactone Composites/Blends and Their Applications Especially in Water Treatment. *ChemEngineering* **2023**, *7*, 104. https://doi.org/10.3390/chemengineering7060104.
72. Thakur, M.; Majid, I.; Hussain, S.; et al. Poly(ε-Caprolactone): A Potential Polymer for Biodegradable Food Packaging Applications. *Packag. Technol. Sci.* **2021**, *34*, 449–461. https://doi.org/10.1002/pts.2572.
73. Carrete, I.A.; Bermudez, D.; Aguirre, C.; et al. Failure Analysis of Additively Manufactured Polyester Test Specimens Exposed to Various Liquid Media. *J. Fail. Anal. Preven.* **2019**, *19*, 418–430. https://doi.org/10.1007/s11668-019-00614-0.
74. Fernández-Tena, A.; Pérez-Camargo, R.A.; Coulembier, O.; et al. Effect of Molecular Weight on the Crystallization and Melt Memory of Poly(ε-Caprolactone) (PCL). *Macromolecules* **2023**, *56*, 4602–4620. https://doi.org/10.1021/acs.macromol.3c00234.
75. Çay, A.; Kumbasar, E.P.A.; Akduman, Ç. Effects of solvent mixtures on the morphology of electrospun thermoplastic polyurethane nanofibres. *Text. Appar.* **2015**, *25*, 38–46.
76. Marșavina, L.; Vălean, C.; Mărghitaș, M.; et al. Effect of the Manufacturing Parameters on the Tensile and Fracture Properties of FDM 3D-Printed PLA Specimens. *Eng. Fract. Mech.* **2022**, *274*, 108766. https://doi.org/10.1016/j.engfracmech.2022.108766.
77. Ćwikła, G.; Grabowik, C.; Kalinowski, K.; et al. The Influence of Printing Parameters on Selected Mechanical Properties of FDM/FFF 3D-Printed Parts. *IOP Conf. Ser. Mater. Sci. Eng.* **2017**, *227*, 012033. https://doi.org/10.1088/1757-899X/227/1/012033.
78. Rodríguez-Reyna, S.L.; Mata, C.; Díaz-Aguilera, J.H.; et al. Mechanical Properties Optimization for PLA, ABS and Nylon + CF Manufactured by 3D FDM Printing. *Mater. Today Commun.* **2022**, *33*, 104774. https://doi.org/10.1016/j.mtcomm.2022.104774.
79. Cojocaru, V.; Frunzaverde, D.; Miclosina, C.-O.; et al. The Influence of the Process Parameters on the Mechanical Properties of PLA Specimens Produced by Fused Filament Fabrication—A Review. *Polymers* **2022**, *14*, 886. https://doi.org/10.3390/polym14050886.
80. The Effect of Processing Parameters on the Mechanical Characteristics of PLA Produced by a 3D FFF Printer|The International Journal of Advanced Manufacturing Technology. Available online: https://link.springer.com/article/10.1007/s00170-020-06138-4 (accessed on 11 November 2025).
81. Peterlin, A. Tensile Failure of Crystalline Polymers. *J. Macromol. Sci. Part B* **1981**, *19*, 401–419. https://doi.org/10.1080/00222348108015311.